The role of microstructural development in the hydrothermal corrosion of cast and HIPed Stellite 6 (S-6) analogues in simulated PWR conditions

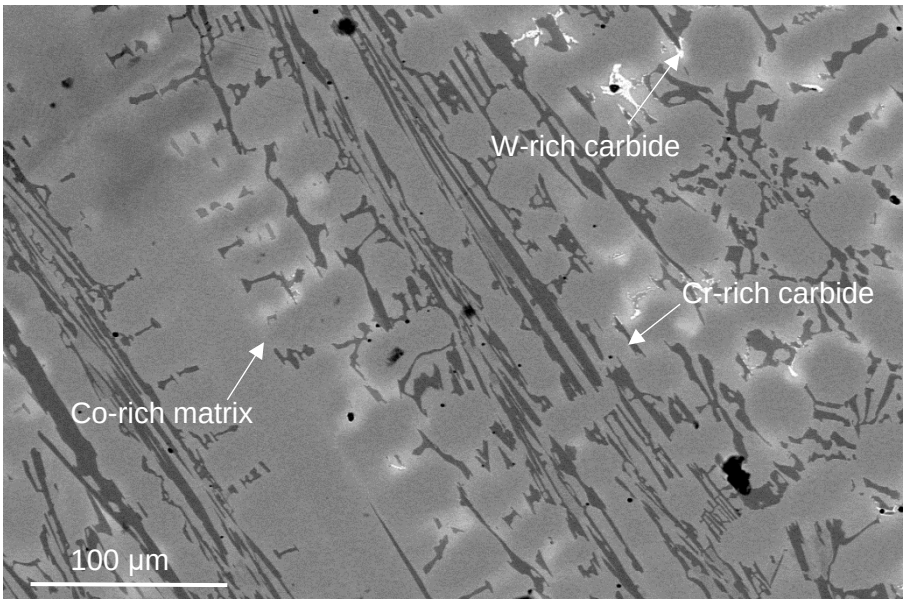

Figure 1. BSE Micrograph of cast S-6 showing the three main phases.

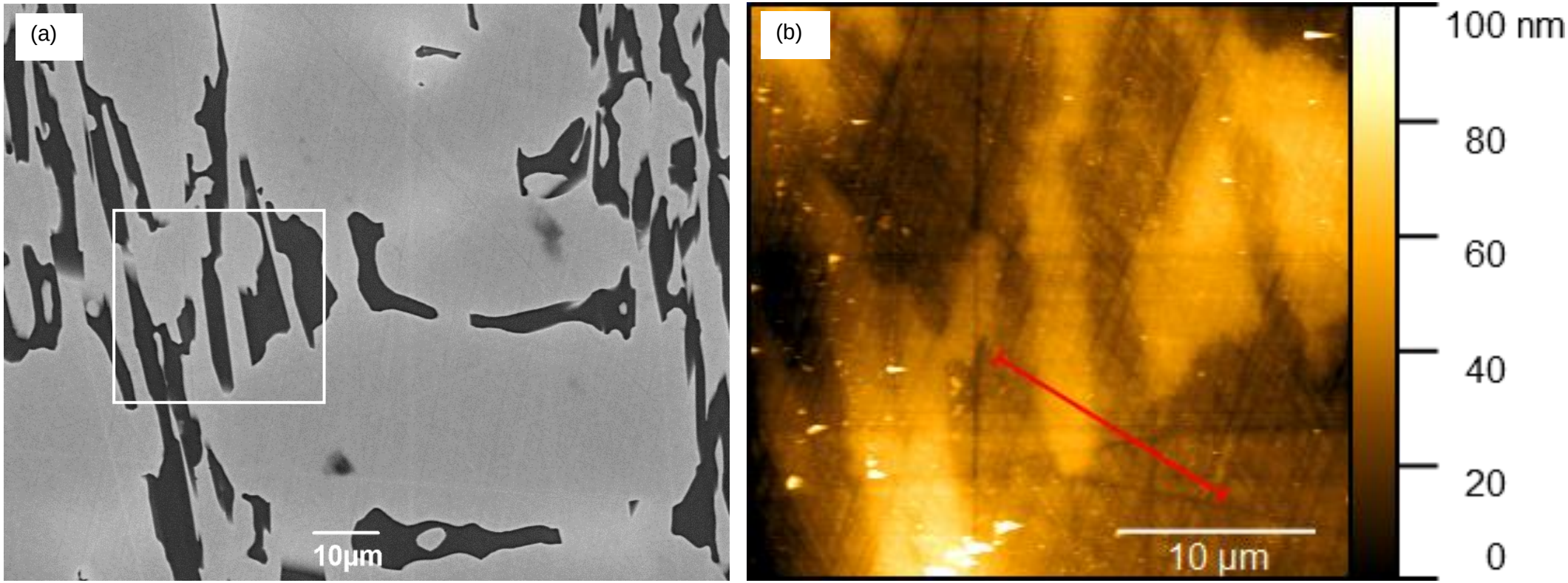

Figure 2. Imaging and analysis of cast S-6 before autoclave exposure: (a) BSE-SEM image with the region where AFM was conducted indicated by a white box; (b) AFM contact-mode height map with a line indicating the position of the height profile presented in Figure 3.

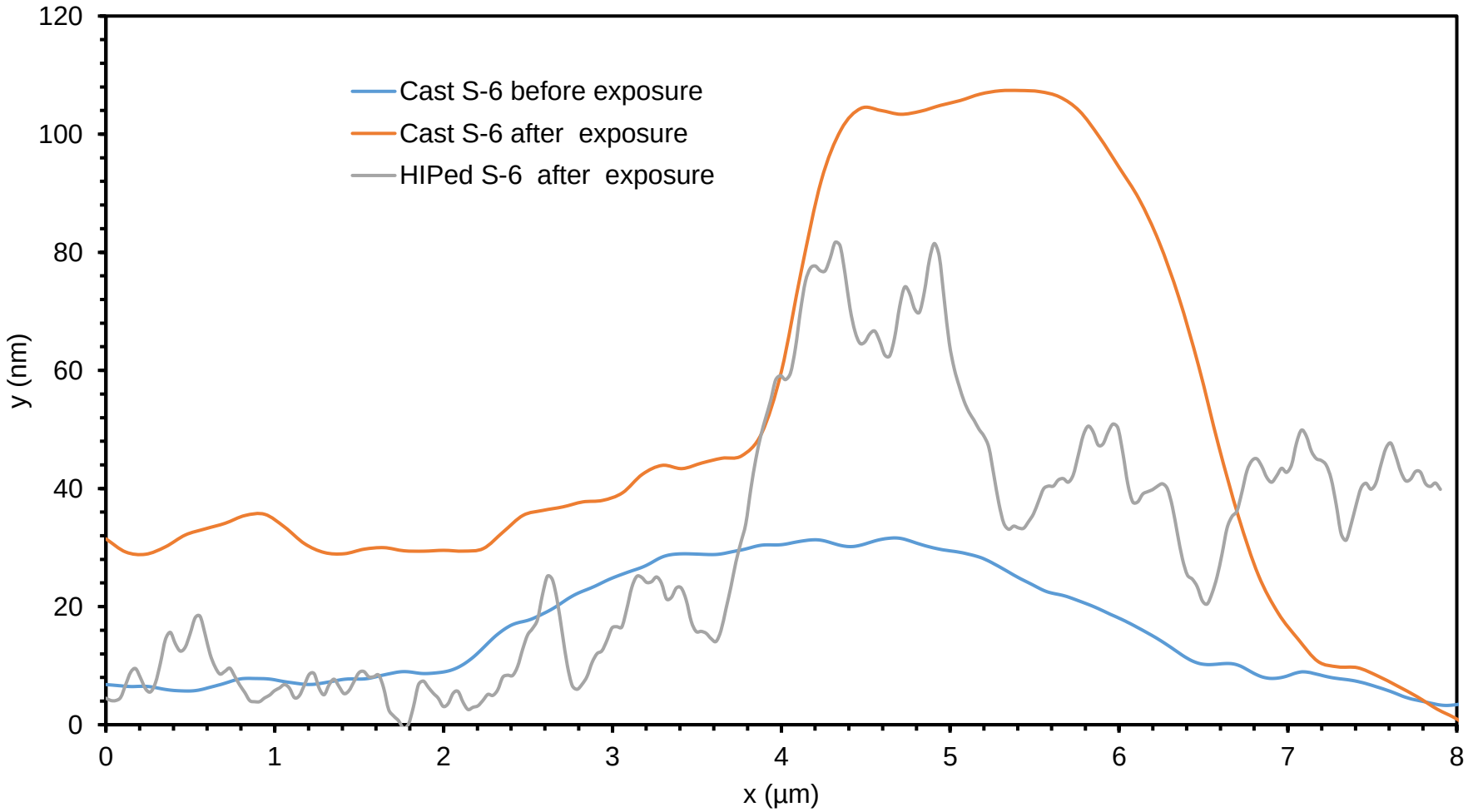

Figure 3. Line profiles from the AFM heights maps showing the height differences between the Co-rich matrix and the Cr-rich carbide in both the cast and HIPed S-6 for the conditions as marked as follows: cast S-6 before exposure (from Figure 2(b); cast S-6 after autoclave exposure (from Figure 7(c)); HIPed S-6 after autoclave exposure (from Figure 11(b).

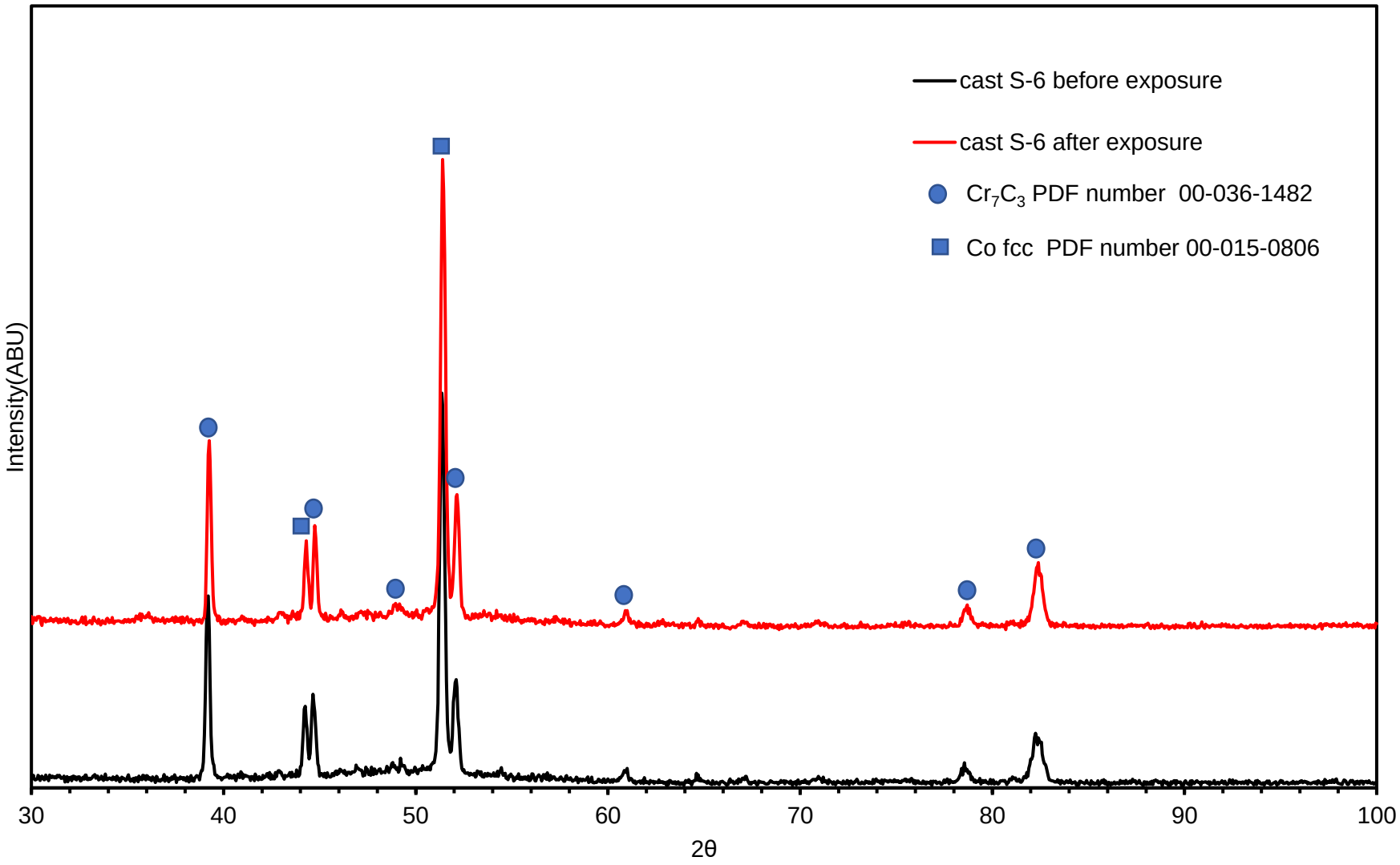

Figure 4. XRD patterns of cast S-6 both before and after autoclave exposure showing peaks associated with the two main phases.

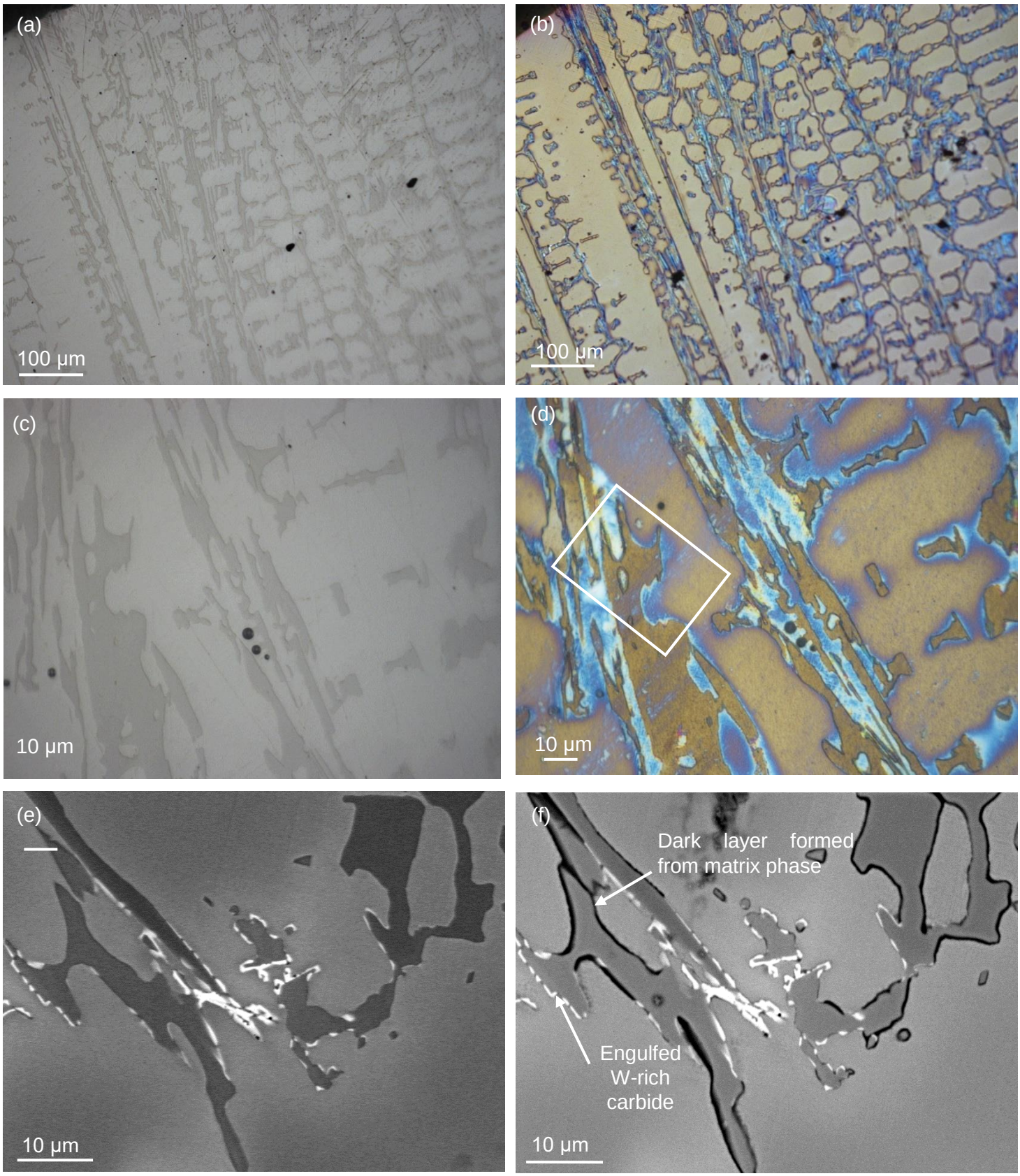

Figure 5. Image pairs of the same regions of cast S-6 before and after autoclave exposure; (a) and (b) low magnification OM images before and after exposure respectively; (c) and (d) high magnification OM images before and after exposure respectively; (e) and (f) BSE-SEM images before and after exposure respectively. The white box in (d) indicates the region where EDX mapping (presented in Figure 6) and AFM mapping (presented in Figure 7) was conducted

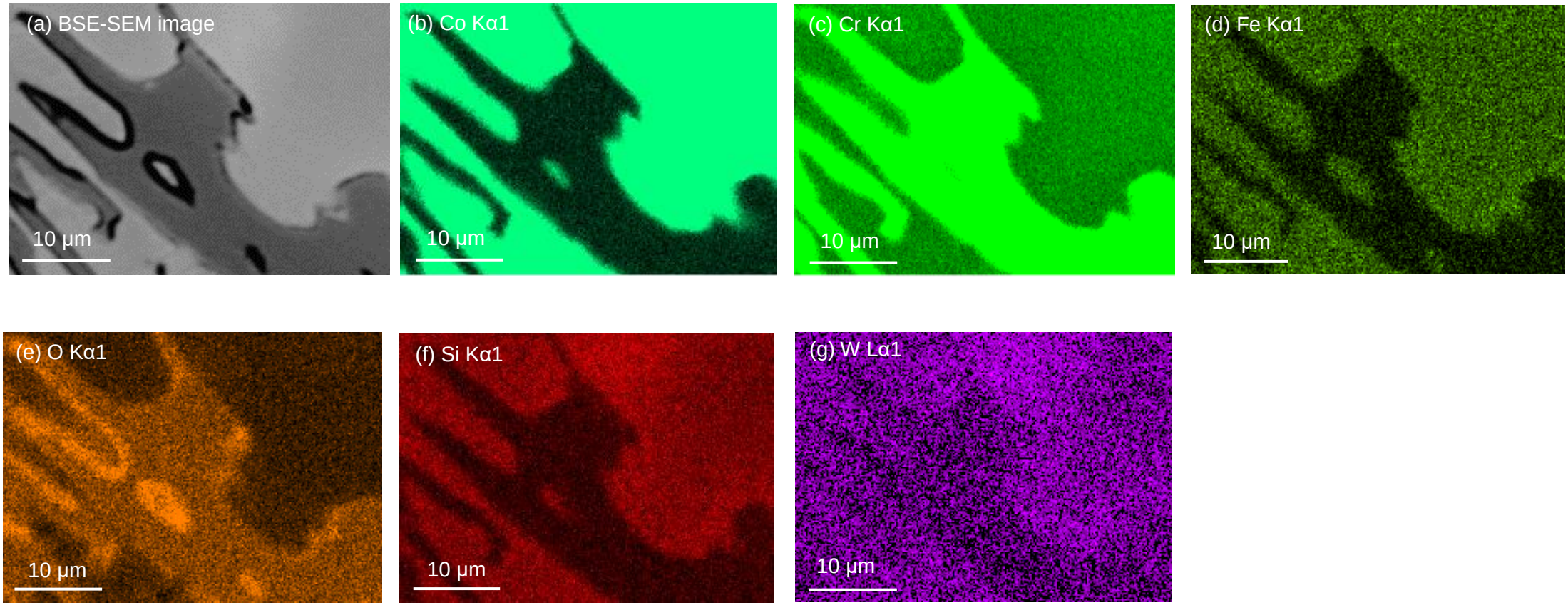

Figure 6. BSE-SEM image and EDX maps of cast S-6 after autoclave exposure examining the region highlighted in Figure 5(d): (a) BSE-SEM image; EDX maps of the following elements: (b) Co Kα1; (c) Cr Kα1; (d) Fe Kα1; (e) O Kα1; (f) Si Kα1; (g) W Lα1

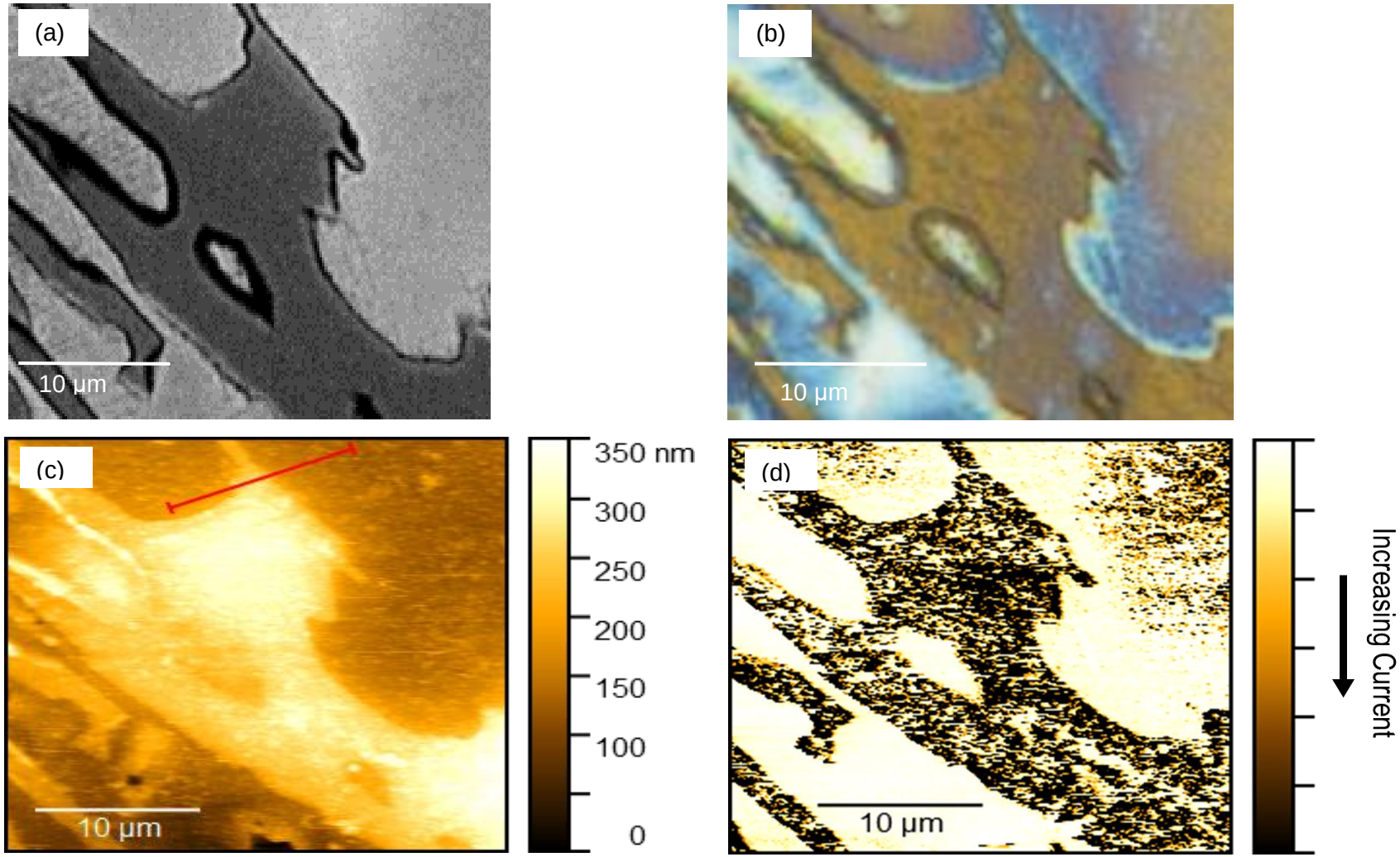

Figure 7. Imaging and analysis of the same region of cast S-6 after autoclave exposure, using a variety of techniques: (a) BSE-SEM image showing interfacial corrosion; (b) optical image showing interference colours associated with the corrosion products, with blue indicating a thicker corrosion product; (c) AFM tapping-mode height map with a line indicating the position of the height profile presented in Figure 3; (d) AFM contact-mode current map showing regions of higher current flow (dark).

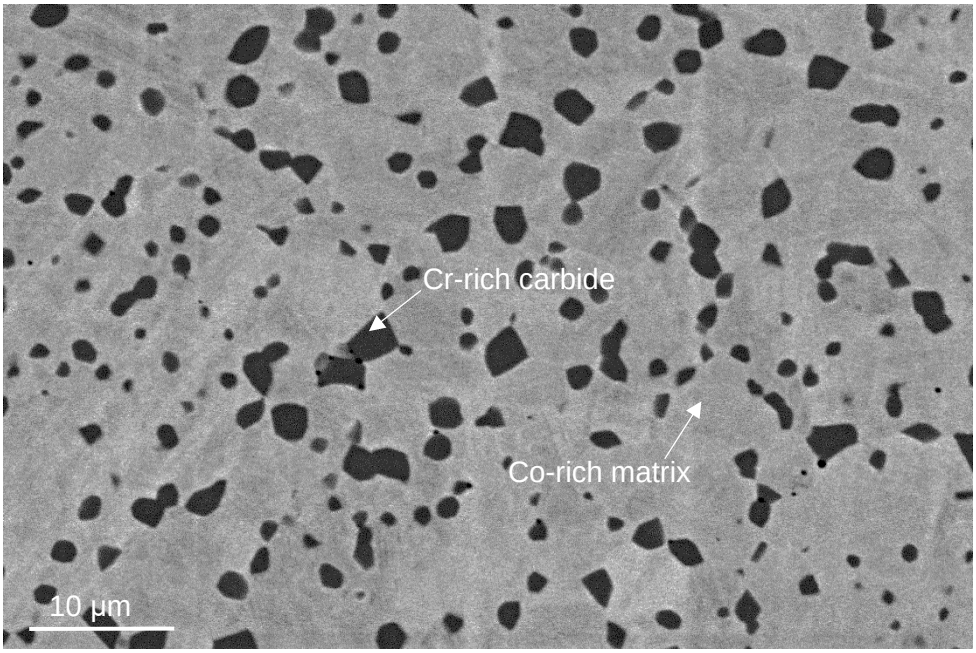

Figure 8. BSE micrograph of HIPed S-6 showing the two main phases.

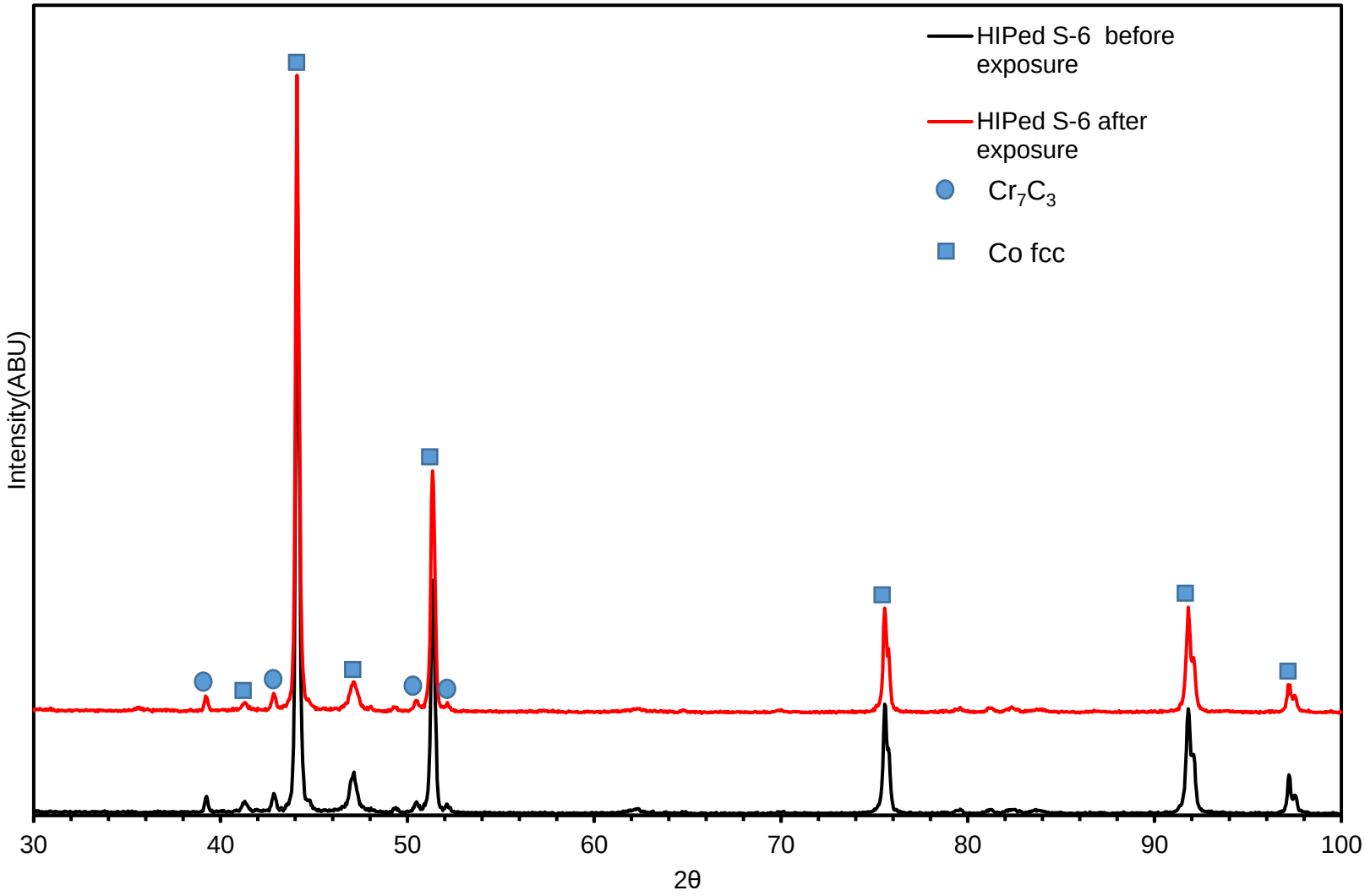

Figure 9. XRD patterns of HIPed S-6 both before and after autoclave exposure showing peaks associated with the two main phases.

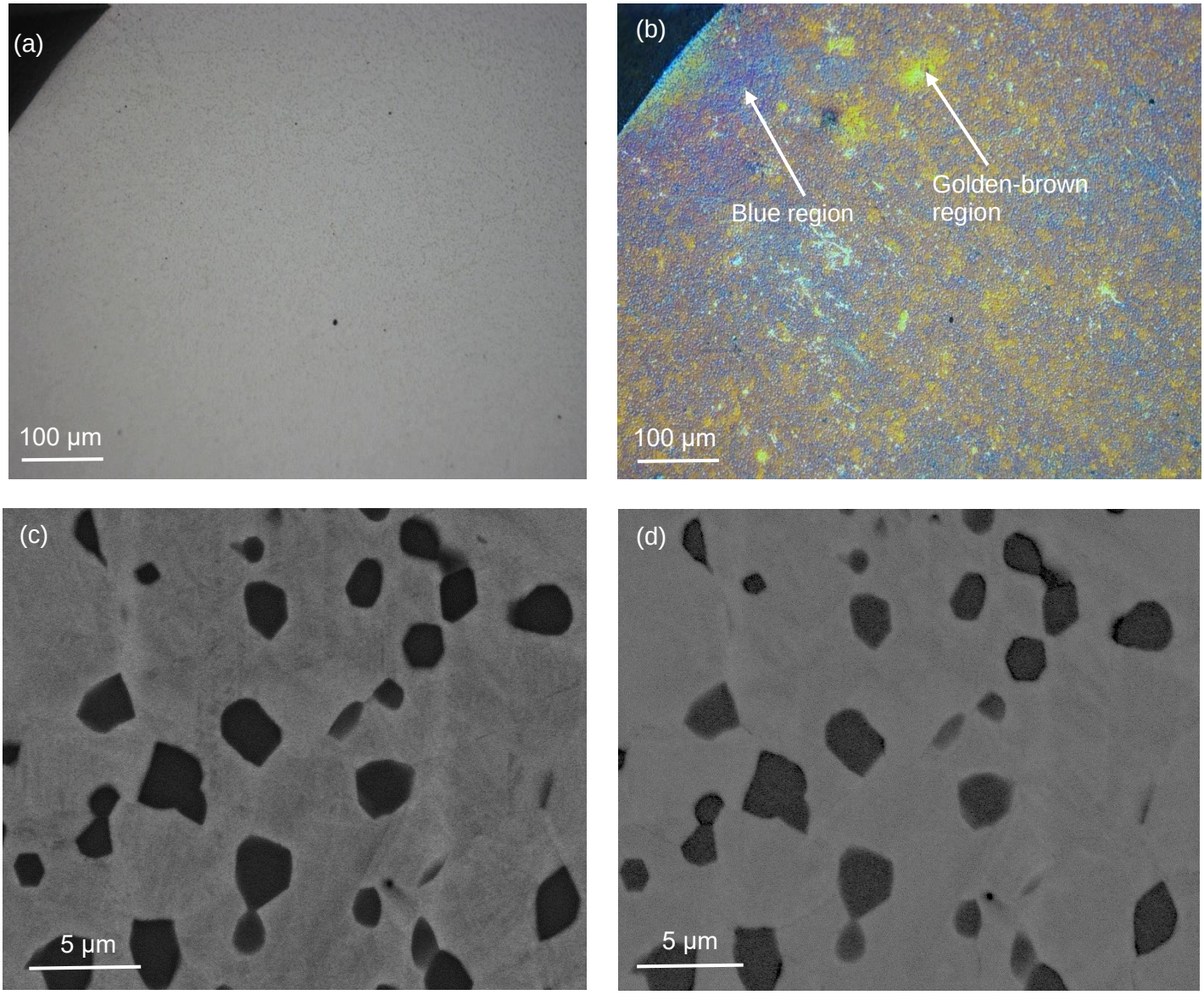

Figure 10. Image pairs of the same regions of HIPed S-6 before and after autoclave exposure; (a) and (b) low magnification OM images before and after exposure respectively; (c) and (d) BSE-SEM images before and after exposure respectively.

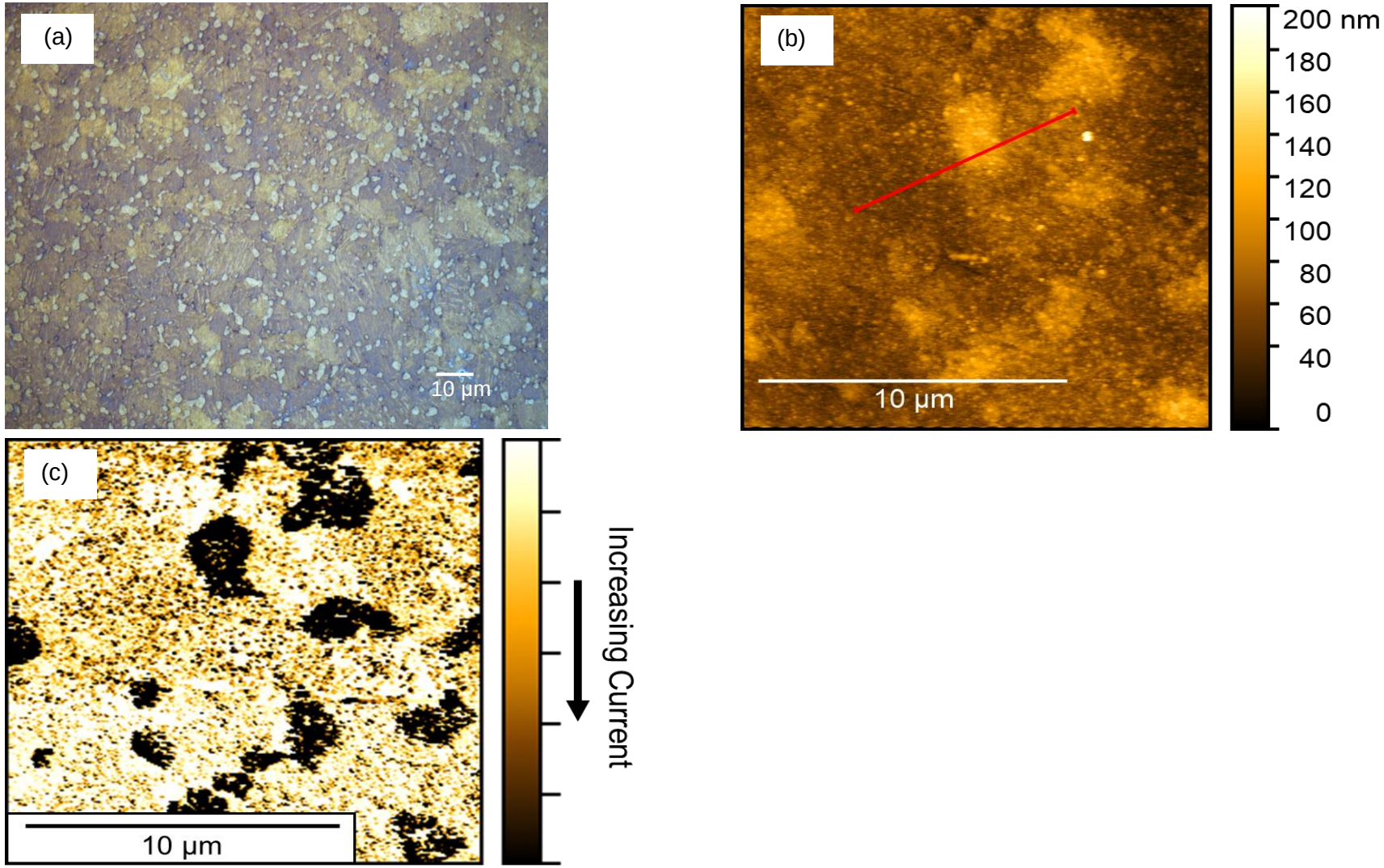

Figure 11. Imaging and analysis of HIPed S-6 after autoclave exposure: (a) optical image showing general region where AFM imaging was performed; (b) AFM tapping-mode height map with a line indicating the position of the height profile across Co-rich matrix with a Cr-rich carbide presented in Figure 3; (c) AFM contact-mode current map of the same area examined in (b).

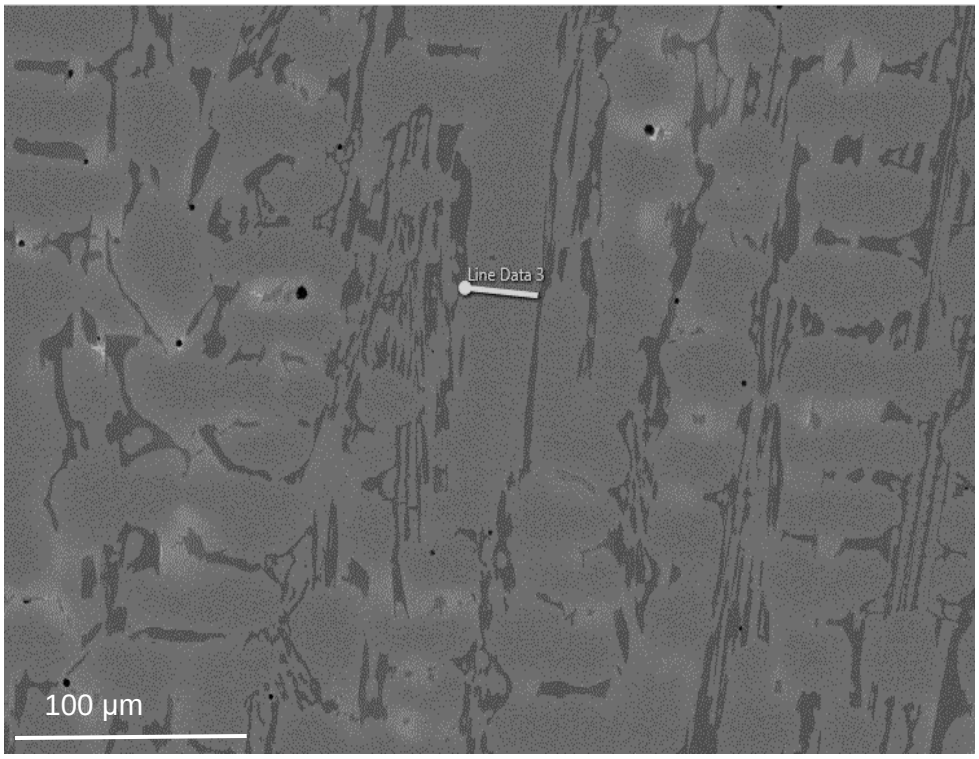

Figure 12(a). BSE image of cast S-6 of showing the line across a dendrite arm along which EDX analysis was made.

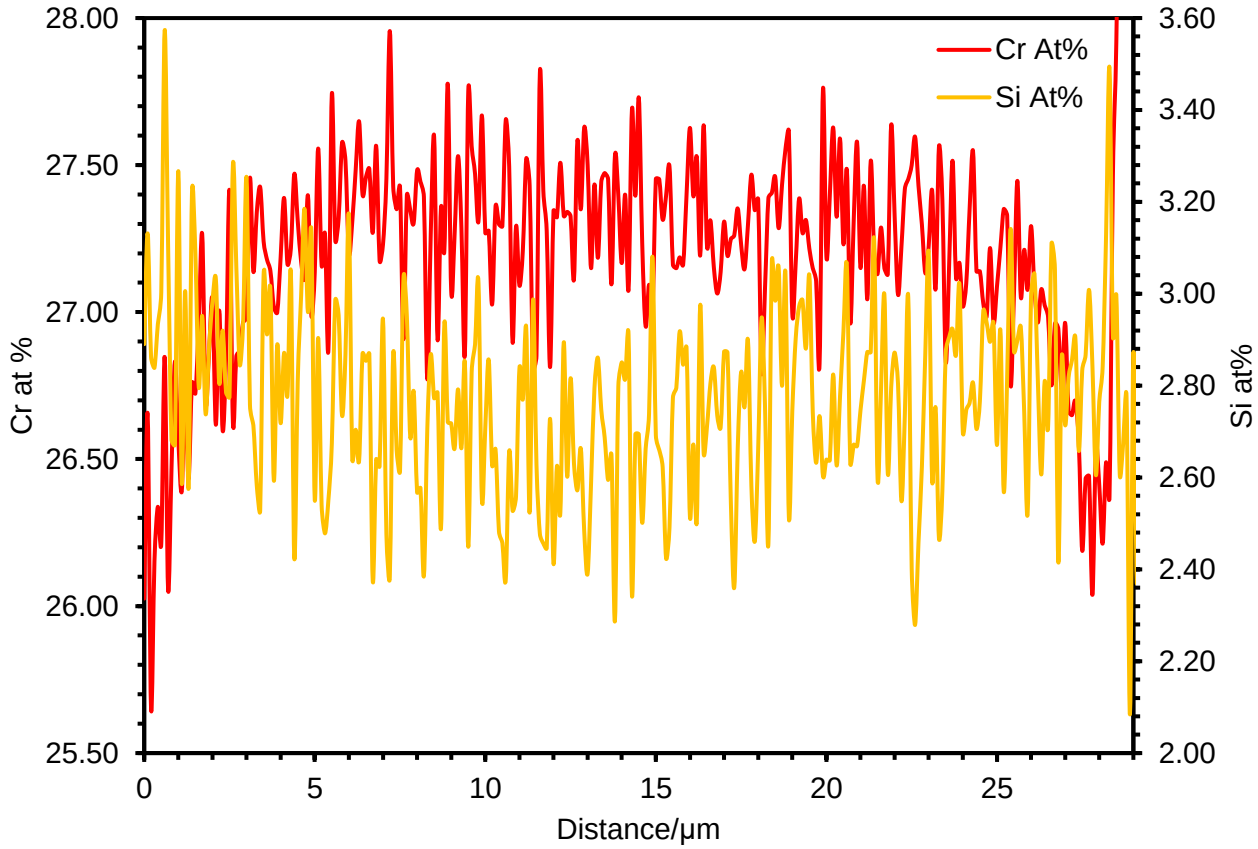

(b) compositions of chromium and silicon measured across the dendrite arm.

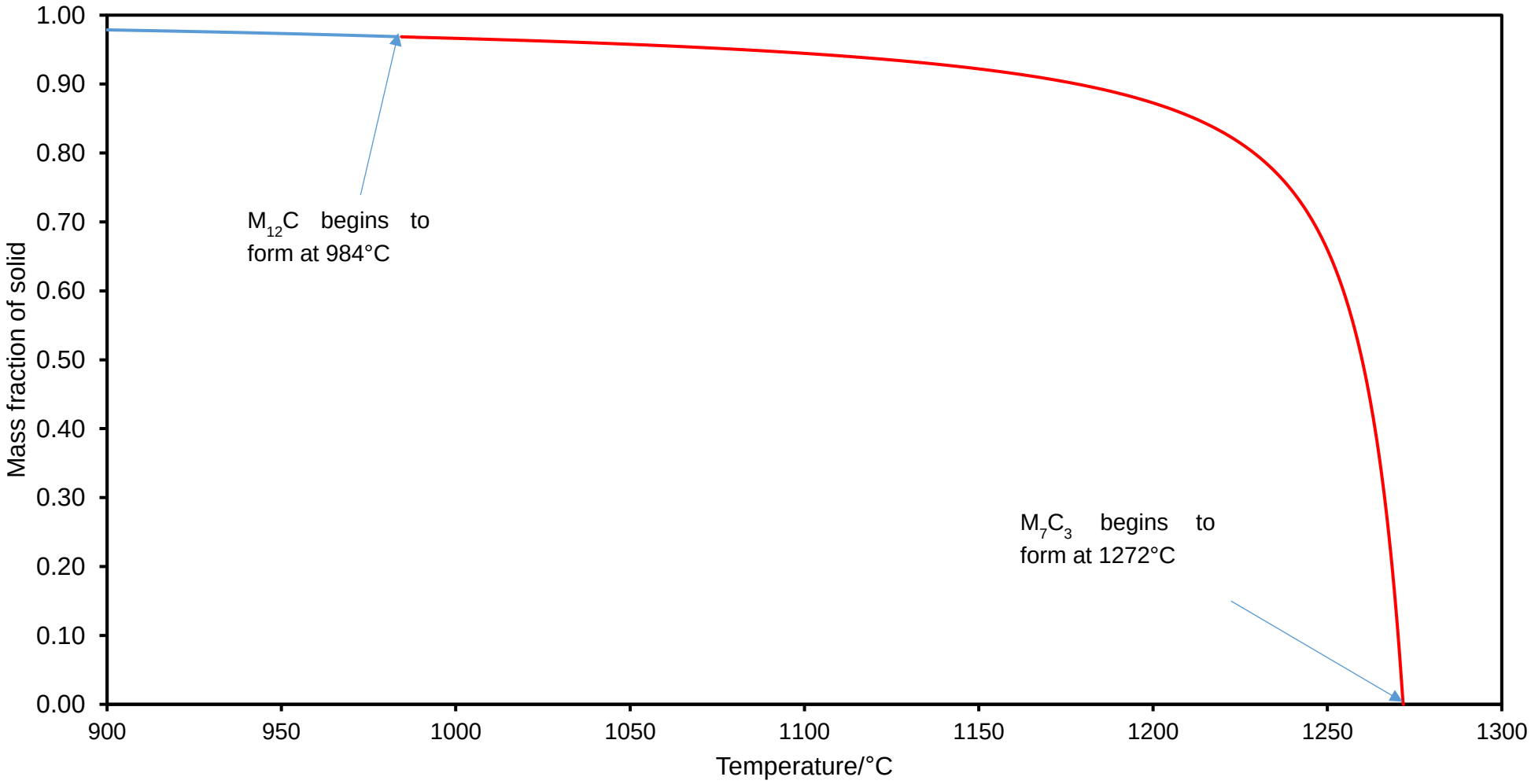

Figure 13(a). Predictions from Scheil–Gulliver solidification modelling of cast S-6: (a) mass fraction of solid as a function of temperature plot showing the temperatures at which particular phases began to be formed during the solidification sequence;

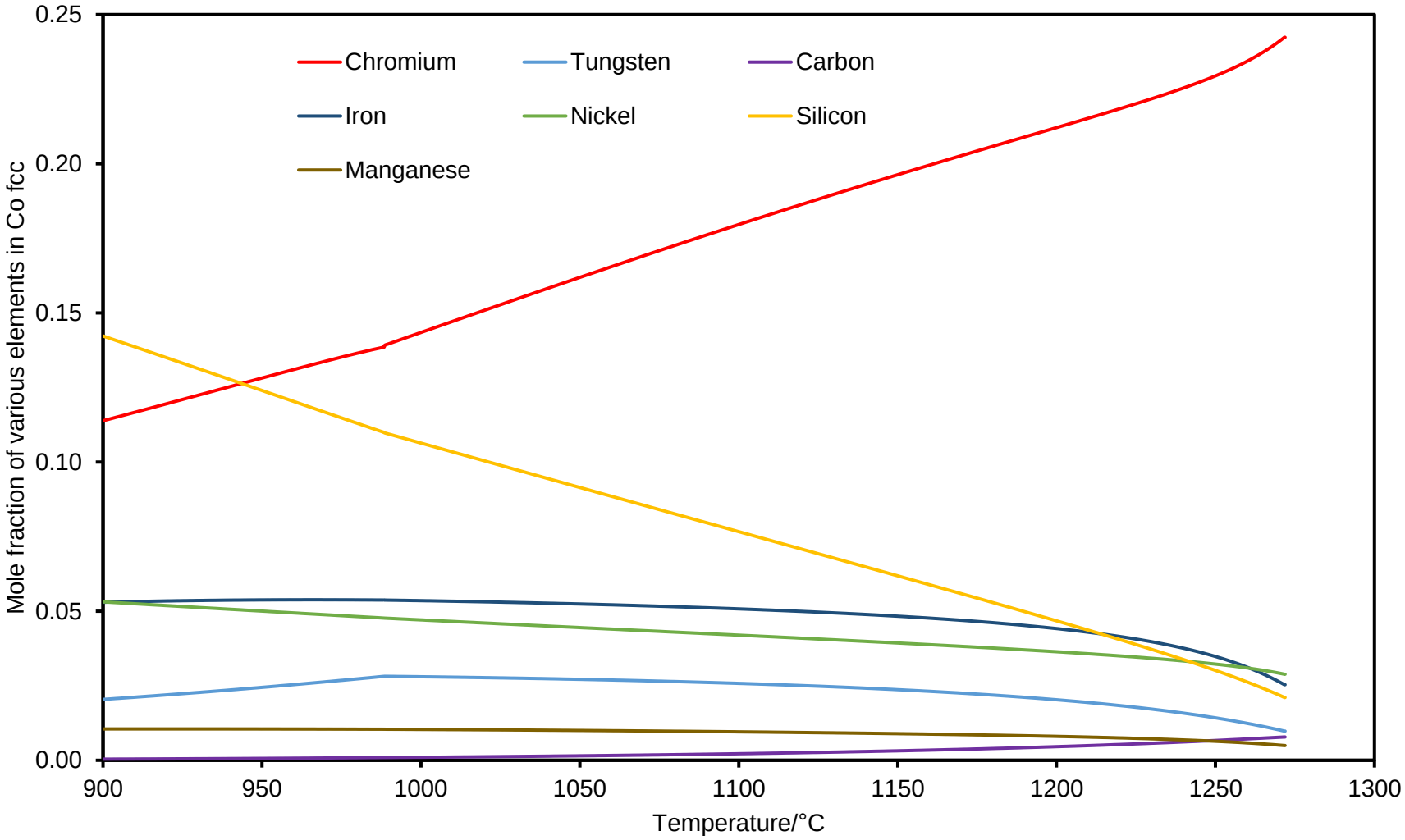

(b). composition of the Co fcc being formed at each temperature as solidification progresses (temperature being reduced

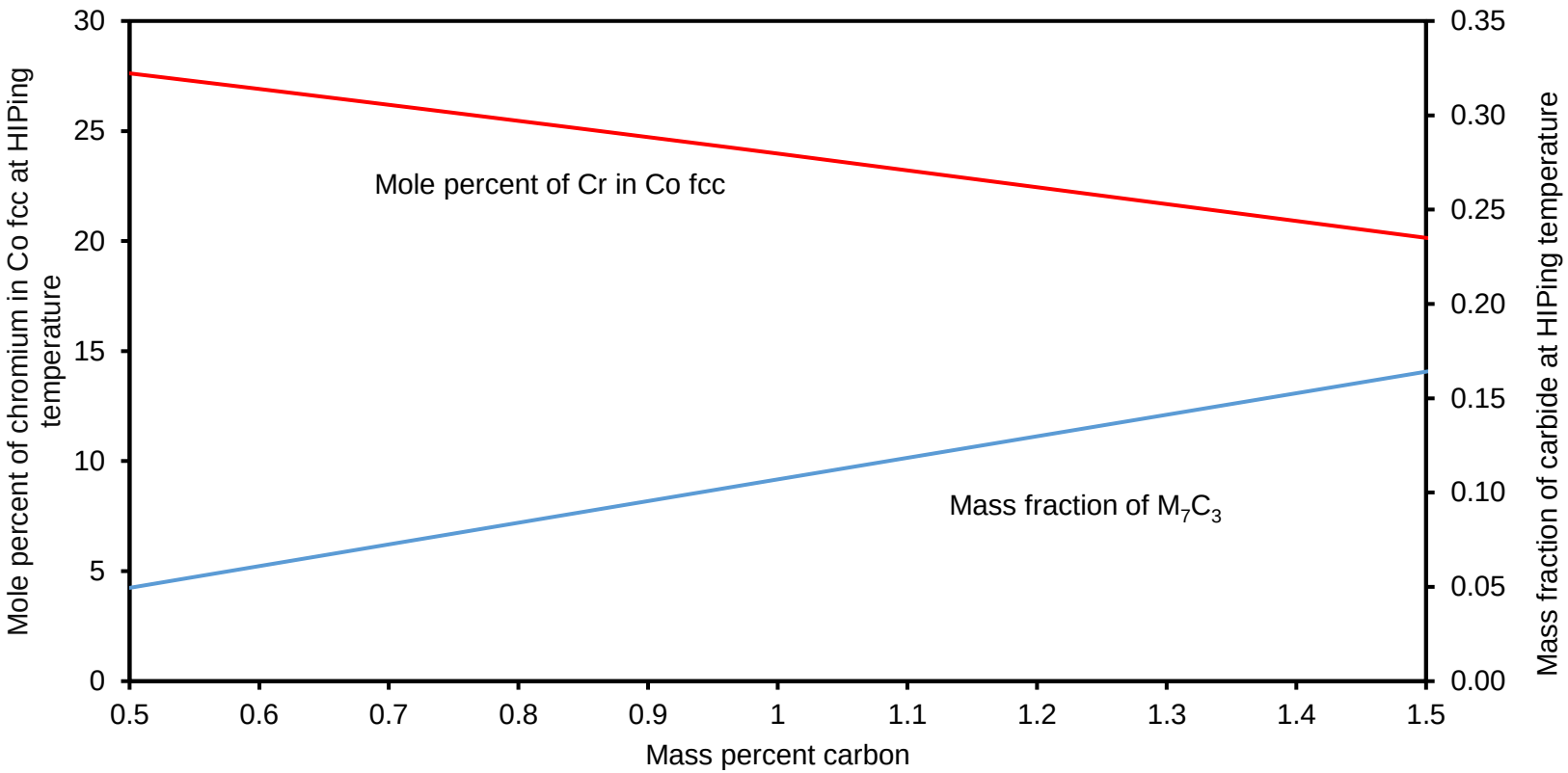

Figure 14. Predictions of variation in features (mass fraction of M_7C_3 and the chromium content in the Co fcc phase) of the equilibrium microstructure at 1200°C in an alloy with the composition of HIPed S-6 but with the carbon level being allowed to vary (at the expense of the cobalt only).